Annealing Effects of Ti/Au Contact on n-MgZnO/p-Si Ultraviolet-B Photodetectors

Yaonan Hou, Zengxia Mei, Huili Liang, Daqian Ye, Changzhi Gu, Xiaolong Du, and Yicheng Lu

Abstract—Effects of postannealing on Ti/Au-MgZnO contact and n-MgZnO/p-Si heterojunction ultraviolet-B photodetector's performance are investigated. It is found that the out diffusion of oxygen from MgZnO and its bonding with Ti at the interface have significant influences on the properties of Ti/MgZnO interface and photodetector. The persistent photocurrent observed in the annealed device is attributed to the oxygen vacancies near the interface, consistent with the theoretical calculations. It is revealed that the reaction at metal/MgZnO interface possibly plays a key role and even dominates the MgZnO p-n heterojunction ultraviolet detectors' performances.

Index Terms—MgZnO, metal-semiconductor contact, persistent photocurrent (PPC), ultraviolet photodetector.

I. INTRODUCTION

AS AN oxide semiconductor material with continuous tunable wide bandgap from 3.37 to 7.8 eV, wurtzite $Mg_xZn_{1-x}O$ (W-$Mg_xZn_{1-x}O$) has demonstrated its versatile functionality in various device application, such as deep ultraviolet (UV) light emitters, UV laser diodes, UV photodetectors (PDs), and 2-D electron gas devices [1]–[5]. The special advantages of $Mg_xZn_{1-x}O$ used in a wide range of UV detection fields, including photolithography, biochemistry, flame/engine control, missile plume detection and covert space-to-space communication, and attract more and more attention recently [6], [7]. Short cutoff wavelength, high photoresponsivity, and fast photoresponse speed are the key targets for applicative UV PDs. To reach this goal, many efforts have been contributed to the synthesis of high-quality W-$Mg_xZn_{1-x}O$ films with high Mg content for the deep UV PD applications.

In our previous research, solar-blind UV detectors based on W-$Mg_{0.55}Zn_{0.45}O$ and W-$Mg_{0.44}Zn_{0.56}O$ epitaxial films were achieved on both sapphire (0001) and Si (111) with the cutoff wavelengths at 270 and 280 nm, respectively,

where the bottleneck of phase segregation in high-Mg content MgZnO was solved by the unique interface engineering techniques [8], [9]. It is well known that a metal–semiconductor (M–S) contact plays an important role in governing the device characteristics, particularly, in PDs. In addition, most of the $Mg_xZn_{1-x}O$-based UV PDs are constructed directly by Schottky-type or ohmic-type metal–semiconductor–metal (MSM) structure. Many excellent device performances, such as low leakage current, high signal-to-noise ratio, large internal gain, and short decay time, can be obtained just by adjusting the contact configuration [10]–[13]. Although it was revealed that the p-n junction of UV PDs has more superior advantages than that of MSM ones according to our previous research [10], the Schottky type M–S contact still can be improved to achieve a higher photoresponsivity. In most cases, thermal annealing is an effective way to change the properties of M–S contact [14]. However, its influences on the device performances have not been studied yet in the MgZnO-based p-n junction UV PDs due to the difficulties in high-Mg content thin film synthesis because of the well-known phase segregation problem [15]. In this paper, Ti/Au contacts on n-$Mg_{0.4}Zn_{0.6}O$/p-Si heterojunction UV-B PDs were constructed, and the influence of annealing on the contacts as well as the device properties was investigated. Ti/Au electrodes were chosen because Ti possesses the merits of both low work function and good adhesion to MgZnO [16].

II. EXPERIMENT

The epitaxial $Mg_{0.4}Zn_{0.6}O$ film was grown on a p-Si (111) substrate by radio frequency plasma-assisted molecular beam epitaxy technique. A BeO interfacial layer and a quasi-homo MgZnO buffer layer with low Mg fraction were adopted to protect the clean Si (111) surface and accommodate the lattice strain, respectively. The quasi-homo MgZnO buffer with low Mg content has a same wurtzite structure and similar lattice constant with the epitaxial layer, which can serve as a good template to suppress phase segregation problem during high-Mg content $Mg_{0.4}Zn_{0.6}O$ growth [17]. The detectors were fabricated by the conventional optical lithography and liftoff procedure. Comblike Ti(10 nm)/Au(60 nm) electrodes were patterned on the W-$Mg_{0.4}Zn_{0.6}O$ epilayer, with each individual teeth 300 μm in length and 5 μm in width. The size of gaps between the tooth is 15 μm (insets of Fig. 1). The electrodes were deposited at room temperature using a thermal evaporator system, with a background pressure of 1×10^{-6} mbar and a deposition rate of 0.05 Å/s. After that, the front electrodes (Ti/Au) were annealed at 400 °C for 10 min in argon atmosphere. It should be noted that growth
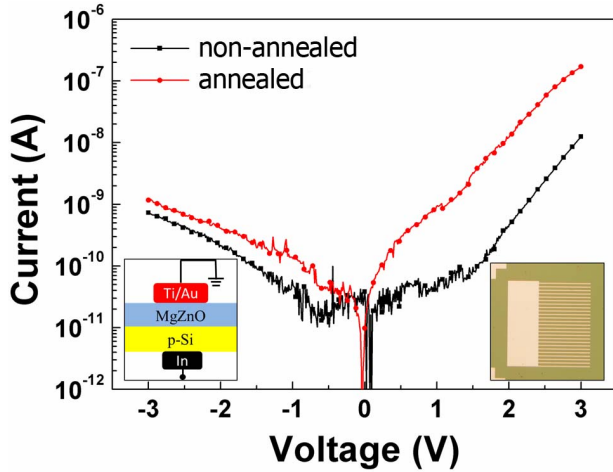
Fig. 1. Dark I–V characteristics of the nonannealed (square) and annealed (dot) Ti/Au-MgZnO/Si heterojunction UV-B PDs (Inset: device structure and the top view of Ti/Au electrodes).

Fig. 2. Spectra response of the nonannealed and annealed UV-B detectors.

of MgZnO was performed at 450 °C, 50 °C higher than the annealing temperature, which guarantees the n-MgZnO/p-Si interface not being damaged during the electrode annealing process. A 2-mm^2 indium was pasted on the back side of p-Si wafer after the removal of SiO$_2$ to form the p-type ohmic contact. The detector performances before and after annealing were characterized. A Keithley 6487 picoammeter was used for the current–voltage (I–V) characterization. Photoresponse properties were obtained using the SpectraPro-500i (Acton Research Corporation) optical system with a 75-W Xe-arc lamp combined with a 0.5-m monochromator as the light source. Time response speed was measured by recording the photocurrent decay behavior generated by periodic 254-nm UV illumination.

III. RESULT AND DISCUSSIONS

The I–V curves of the as-fabricated (labeled as nonannealed) and annealed (labeled as annealed) UV PDs are shown in Fig. 1. Through fitting the curves with Sah–Noyce–Shockley model, we got an ideality factor of eight for the nonannealed and 12 for the annealed detectors, respectively. Such large ideal factors are induced by the electron tunneling through the large Schottky barrier formed by Ti/Au contact on MgZnO, considering that In electrodes on Si is ohmic (not shown here).

This high Schottky barrier is closely related with the energy band structure of Mg$_{0.4}$Zn$_{0.6}$O film. When Mg atoms are incorporated into ZnO, the Mg 3s-electron will sufficiently lift the conduction band minimum (CBM) of MgZnO leaving the valence band maximum hardly moved, with a ratio of ΔE_C:ΔE_V up to 9:1 [10]. Therefore, the electron affinity of W-Mg$_{0.4}$Zn$_{0.6}$O is reduced to a smaller value compared with that of pure ZnO. According to Schottky–Mott theory, a large barrier will be introduced near Ti/MgZnO interface. The tunneling of electrons through this large barrier leads to a large ideality factor. It can be seen that the dark current at -3 V increases slightly from 7×10^{-10} to 1.9×10^{-9} A after annealing, which will be discussed in the later part.
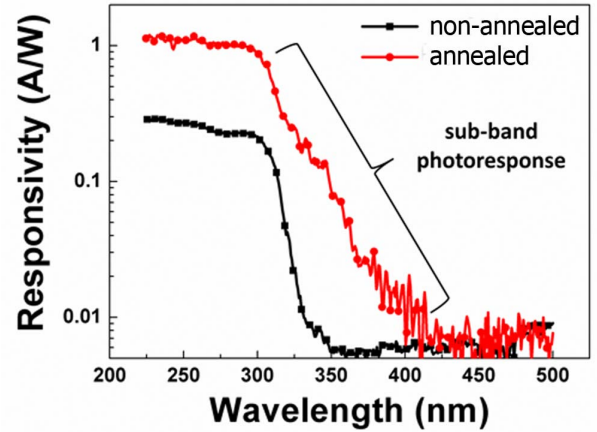
Spectra response curves of the nonannealed and annealed detectors at -2 V bias are shown in Fig. 2. The cutoff wavelength of both detectors clearly locates at 300 nm with a similar UV/visible light rejection ratio of two orders of magnitude, suitable for UV-B ($\lambda < 320$ nm) detection. Compared with the nonannealed detector, the responsivity of the annealed detector increases from 0.22 to 1 A/W, and a subband response emerges between 300 and 400 nm. These changes can be understood by considering the reaction between Ti and O at the Ti/MgZnO interface during the annealing process in the following part.

Since Ti has a lower enthalpy with O atom than that of Mg and Zn (ΔH_f^o(TiO$_2$) = -944 kJ/mol, ΔH_f^o (MgO) = -601 kJ/mol, and ΔH_f^o (ZnO) = -350 kJ/mol), Ti will preferentially bond with O atoms out diffused from the MgZnO caused by annealing, generating many oxygen vacancies which act as deep level donors in MgZnO [18]. To prove our argument, Raman spectra (Fig. 3) measurements were carried out and studied at room temperature with a 532-nm laser illuminating on the electrodes (the diameter of laser spot is 5 μm). Although the Raman signals fall in a strong background introduced by the PL signals from Si substrate, Raman scattering peaks still can be easily recognized. Considering the stress change in ZnO lattice induced by the incorporation of Mg atoms, it is reasonable to attribute the peaks at 90, 447, and 402 cm^{-1} to E_2^{low}, E_2^{high}, and E_1(TO) modes of MgZnO, respectively. The peaks at 135 and 215 cm^{-1} are identified as E_g(1) and E_g(2) modes of TiO$_x$, while 522 cm^{-1} is composed of A$_1$(g)+B$_1$(g) from TiO$_x$ [19]. For comparison, the E_2^{low} peaks of MgZnO before and after annealing were normalized for reference. It can be clearly seen that the E_g(1), E_g(2), and A$_1$(g)+B$_1$(g) peaks of the annealed detector are obviously enhanced compared with those of the nonannealed, indicating the occurrence of Ti-O bonding at the Ti/MgZnO interface during the annealing process. The increment of the darkcurrent and photocurrent (photoresponsivity) of the annealed detector (Figs. 1 and 2) results from this kind of ohmic contact metallization. Simultaneously, Urbach tail [20], which is represented by the subband photoresponse shown in Fig. 2, forms due to the high density of intrinsic defects.
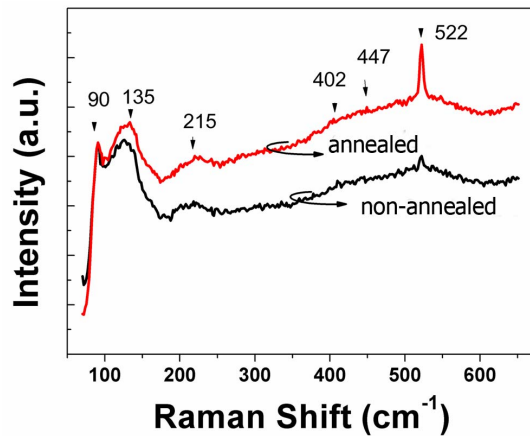
Fig. 3.   Raman spectra of the nonannealed (black line) and annealed (red line) UV-B detectors, and the peaks from TiO$_x$ are marked out.

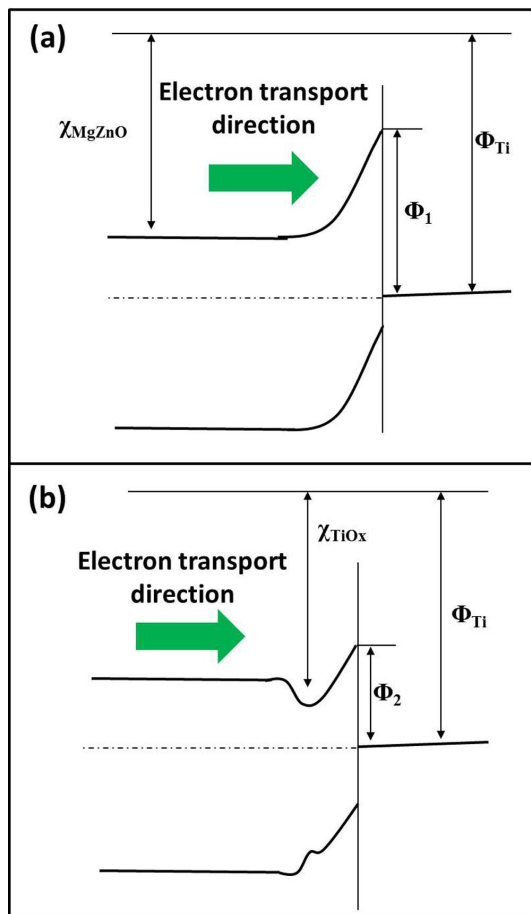
Fig. 4.   Energy band diagrams of Ti/MgZnO interface (a) before annealing and (b) after annealing.

The value of Urbach energy (E_U) is determined as 240 meV by fitting E_U with the equation of $R = R_0 \exp(E_{hv}/E_U)$. It is known that the Urbach energy increases along with structural disorder, therefore such a large value indicates the occurrence of a disordered state induced by annealing process near the Ti/MgZnO interface in MgZnO epilayer.

In addition, the electron affinity of TiO$_x$ is larger than that of Mg$_{0.4}$Zn$_{0.6}$O, while the bandgap is smaller [21].
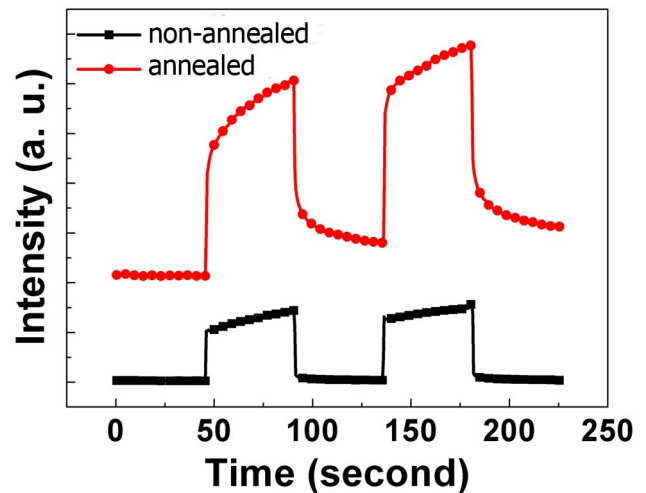

Fig. 5.   Comparison of response speeds of the nonannealed and annealed UV-B detectors.

As the Schottky barrier height is defined as $\Phi = \Phi_m - \chi_s$, the Schottky barrier height of the annealed detectors is lower than that of the nonannealed, as shown in Fig. 4. Under reverse bias, the tunneling probability of photogenerated electrons in the annealed detectors is much higher than that of the nonannealed. Therefore, a large responsivity was observed in the annealed detector. The dark current can be explained in a similar fashion.

Time-resolved photocurrent measurements of the two detectors are shown in Fig. 5. The 10%–90% photocurrent decay time of the nonannealed device is ∼1 s. The decay time of the annealed detector is, however, nearly 100 s and the current can hardly reset to its initial value, nominally the persistent photocurrent (PPC). PPC is frequently observed in ZnO/or other wide bandgap semiconductor optoelectronic devices or both. The origin of PPC effect is, however, still a controversy. In general, three mechanisms have been considered: 1) oxygen chemical adsorption and desorption on the surface of the device by trapping electrons or recombining electrons with holes [22]; 2) negatively charged interface states trapping/releasing photogenerated holes [23]; and 3) a complex process closely related to the deep level defects of the semiconductor [24]. Our previous research proved that the surface chemical adsorption is not the key role for PPC [10], and oxygen vacancy (or ionized oxygen vacancy) cannot trap holes. Therefore, the situations 1) and 2) are excluded. We ascribe the prominent PPC effect in the annealed detector to the deep level defects of oxygen vacancies, which can be deduced from the enhanced TiO$_x$ Raman signals and Ti-O bonding. The model proposed by [24] can be applied to well explain why oxygen vacancy defects will induce PPC effect.

In MgZnO, oxygen vacancies often present in three different charge states of V_O^0, V_O^+, and V_O^{++}. According to the calculation, both V_O^0 and V_O^+ are deep level states under CBM that cannot be excited at room temperature and thus have no contribution to the conductivity. Under UV illumination, however, V_O^0 and V_O^+ will be excited to V_O^{++} state by $V_O \rightarrow V_O^{++} + 2e$

and $V_O^+ \rightarrow V_O^{++} + e$. The photogenerated electrons will relax to the conduction band edge and occupy a perturbed host state from V_O^{++} which is a resonant state within the host bands (over CBM), resulting in a photoconduction. Meanwhile, Zn–Zn distance near the oxygen vacancy increases (from ~ 0.3 nm for V_O^0 to ~ 0.37 nm for V_O^{++} in the case of pure ZnO) [24]. The lattice change will introduce an energy barrier (~ 0.2 eV in ZnO) against the depopulation of electrons from metastable state to deep ground V_O^0 state when the light is off. This will lead to a long time for photocurrent relaxation, producing the PPC effect.

IV. CONCLUSION

The annealing effects on the Ti/Au contact and n-MgZnO/p-Si heterojuncton UV-B PDs were investigated through the comparison of electrical properties and photoresponse performance. The value of responsivity was found increased, but the dark current, cutoff edge, and photocurrent decay time degenerated, indicating some adverse effects of the annealing on detector performance. These phenomena were attributed to the out diffusion of oxygen from MgZnO and its bonding with Ti at the interface, which was confirmed by the enhanced TiO$_x$ Raman signals. This paper revealed that the M–S contact plays a critical role in MgZnO p-n heterojunction UV PDs, and significantly influences the device performances.

REFERENCES

[1] P. Chen, X. Ma, D. Li, Y. Zhang, and D. Yang, "Bidirectional direct-current electroluminescence from i-Mg$_x$Zn$_{1-x}$O/n-ZnO/SiO$_x$ double-barrier heterostructures on Si," *Appl. Phys. Lett.*, vol. 94, no. 6, pp. 061110–061112, Feb. 2009.

[2] Y.-S. Tsai and J.-Z. Chen, "Positive gate-bias temperature stability of RF-sputtered Mg$_{0.05}$Zn$_{0.95}$O active-layer thin film transistors," *IEEE Trans. Electron Devices*, vol. 59, no. 1, pp. 151–158, Jan. 2012.

[3] C.-I. Huang, H.-A. Chin, Y.-R. Wu, I.-C. Cheng, J. Z. Chen, K.-C. Chiu, and T.-S. Lin, "Mobility enhancement of polycrystalline MgZnO/ZnO thin film layers with modulation doping and polarization effects," *IEEE Trans. Electron Devices*, vol. 57, no. 3, pp. 696–703, Mar. 2010.

[4] A. Gold, "Transport properties of electron gas in ZnO/MgZnO heterostructures," *Appl. Phys. Lett.*, vol. 96, no. 24, pp. 242111–242113, Jun. 2010.

[5] A. Tsukazaki, S. Akasaka, K. Nakahara, Y. Ohno, H. Ohno, D. Maryenko, A. Ohtomo, and M. Kawasaki, "Observation of fractional quantum Hall effect in an oxide," *Nature Mater.*, vol. 9, pp. 889–893, Oct. 2010.

[6] F. J. Liu, Z. F. Hu, L. Zhu, Z. J. Li, H. Q. Huang, J. W. Zhao, X. Q. Zhang, and Y. S. Wang, "Solar-blind photoresistors based on Mg$_{0.48}$Zn$_{0.52}$O thin films grown on r-Al$_2$O$_3$ substrates by radio-frequency plasma-assisted molecular beam epitaxy," *IEEE Trans. Electron Devices*, vol. 59, no. 7, pp. 1970–1973, Jul. 2012.

[7] Q. Zheng, F. Huang, J. Huang, Q. Hu, D. Chen, and K. Ding, "High-responsivity solar-blind photodetector based on Mg$_{0.46}$Zn$_{0.54}$O thin film," *IEEE Electron Device Lett.*, vol. 33, no. 7, pp. 1033–1035, Jul. 2012.

[8] H. L. Liang, Z. X. Mei, Q. H. Zhang, L. Gu, S. Liang, Y. N. Hou, D. Q. Ye, C. Z. Gu, R. C. Yu, and X. L. Du, "Interface engineering of high-Mg-content MgZnO/BeO/Si for p-n heterojunction solar-blind ultraviolet photodetectors," *Appl. Phys. Lett.*, vol. 98, no. 22, pp. 221902–221904, May 2011.

[9] Y. N. Hou, Z. X. Mei, H. L. Liang, D. Q. Ye, S. Liang, C. Z. Gu, and X. L. Du, "Comparative study of n-MgZnO/p-Si ultraviolet-B photodetector performance with different device structures," *Appl. Phys. Lett.*, vol. 98, no. 26, pp. 263501–263503, Jun. 2011.

[10] Y. N. Hou, Z. X. Mei, Z. L. Liu, T. C. Zhang, and X. L. Du, "MgZnO solar-blind ultraviolet detector with high photoresponse performance and large internal gain," *Appl. Phys. Lett.*, vol. 98, no. 10, pp. 103506–103508, Mar. 2011.

[11] L. K. Wang, Z. G. Zhu, J. Y. Zhang, J. Zheng, D. Z. Shen, B. Yao, D. X. Zhao, Z. Z. Zhang, B. H. Li, and C. X. Shan, "Single-crystalline cubic MgZnO films and their applications in deep-ultraviolet optoelectronic devices," *Appl. Phys. Lett.*, vol. 95, no. 13, pp. 131113–131115, Oct. 2009.

[12] G. Tabares, A. Hierro, J. M. Ulloa, A. Guzman, E. Monze, A. Nakamura, T. Hayashi, and J. Temmyo, "High responsivity and internal gain mechanisms in Au-ZnMgO Schottky photodiodes," *Appl. Phys. Lett.*, vol. 96, no. 10, pp. 101112–101115, Mar. 2010.

[13] S. Han, Z. Zhang, J. Zhang, L. Wang, J. Zheng, H. Zhao, Y. Zhang, M. Jiang, S. Wang, D. Zhao, C. Shan, B. Li, and D. Shen, "Photoconductive gain in solar-blind ultraviolet photodetector based on Mg$_{0.52}$Zn$_{0.48}$O thin films," *Appl. Phys. Lett.*, vol. 99, no. 24, pp. 242105–242108, Dec. 2011.

[14] J. J. Chen, S. Jang, T. J. Anderson, F. Ren, Y. Li, H. S. Kim, B. P. Gila, D. P. Norton, and S. J. Pearton, "Low specific contact resistance Ti/Au contacts on ZnO," *Appl. Phys. Lett.*, vol. 88, no. 12, pp. 122107–122110, Mar. 2006.

[15] X. L. Du, Z. X. Mei, Z. L. Liu, Y. Guo, T. C. Zhang, Y. N. Hou, Z. Zhang, Q. K. Xue, and A. Y. Kuznetsov, "Controlled growth of high-quality ZnO-based films and fabrication of visible-blind and solar-blind ultra-violet detectors," *Adv. Mater.*, vol. 21, no. 45, pp. 4625–4630, Dec. 2009.

[16] W. Lim, D. P. Norton, J. H. Jang, V. Craciun, S. J. Pearton, and F. Ren, "Carrier concentration dependence of Ti/Au specific contact resistance on n-type amorphous indium zinc oxide thin films," *Appl. Phys. Lett.*, vol. 92, no. 12, pp. 122102–122104, Mar. 2008.

[17] Z. L. Liu, Z. X. Mei, T. C. Zhang, Y. P. Liu, Y. Guo, X. L. Du, A. Hallen, J. J. Zhu, and A. Y. Kuznetsov, "Solar-blind 4.55 eV band gap Mg$_{0.55}$Zn$_{0.45}$O components fabricated using quasi-homo buffers," *J. Crystal Growth*, vol. 311, no. 18, pp. 4356–4359, 2009.

[18] L. J. Brillson and Y. Lu, "ZnO Schottky barriers and Ohmic contacts," *J. Appl. Phys.*, vol. 109, no. 12, pp. 121301–121333, Jun. 2011.

[19] H. C. Choi, Y. M. Jung, and S. B. Kim, "Size effects in Raman spectra of TiO$_2$ nanopaticles," *Vibrat. Spectrosc.*, vol. 37, no. 1, pp. 33–38, Jan. 2005.

[20] K. Boubaker, "A physical explanation to the controversial Urbach tailing universality," *Eur. Phys. J. Plus*, vol. 126, pp. 10–14, Jan. 2011.

[21] N. Fuke, A. Fukui, A. Islam, R. Komiya, R. Yamanaka, H. Harima, and L. Han, "Influence of TiO$_2$/electrode interface on electron transport properties in back contact dye-sensitized solar cells," *Solar Energy Mater. Solar Cells*, vol. 93, nos. 6–7, pp. 720–724, Jun. 2009.

[22] C. Soci, A. Zhang, B. Xiang, S. A. Dayeh, D. P. R. Aplin, J. Park, X. Y. Bao, Y. H. Lo, and D. Wang, "ZnO nanowire UV photodetectors with high internal gain," *Nano Lett.*, vol. 7, no. 4, pp. 1003–1009, Mar. 2007.

[23] O. Katz, G. Bahir, and J. Salzman, "Persistent photocurrent and surface trapping in GaN Schottky ultraviolet detectors," *Appl. Phys. Lett.*, vol. 84, no. 20, pp. 4092–4094, May 2004.

[24] S. Lany and A. Zunger, "Anion vacancies as a source of persistent photoconductivity in II–VI and chalcopyrite semiconductors," *Phys. Rev. B*, vol. 72, no. 3, pp. 035215–035227, Jul. 2005.

Authors' photographs and biographies not available at the time of publication.